EXPERIMENTAL EVALUATION OF THE STABILITY AND MECHANICAL BEHAVIOR OF CONTACTS IN SILICON CARBIDE FOR THE DESIGN OF THE BASIC ANGLE MONITORING SYSTEM OF GAIA

A.A. van Veggel[(1)], W.J. Berkhout[(1)], M.K. Schalkx[(1)], A.A. Wielders[(2)], P.C.J.N.Rosielle[(1)], H. Nijmeijer[(1)]

[(1)] Technische Universiteit Eindhoven, Department of Mechanical Engineering, P.O. box 513, 5600 MB Eindhoven, The Netherlands, E-mail: A.A.v.Veggel@tue.nl

[(2)] TNO Science and Industry, Division Opto-Mechanical Instrumentation, P.O. box 155, 2600 AD Delft, The Netherlands

ABSTRACT

The satellite GAIA will be launched in ca. 2010 to make a 3-D map of our Galaxy. The payload module of the satellite will carry two astrometric telescopes amongst other instrumentation. The optical bench and astrometric telescopes will be constructed for a large part in Silicon Carbide (SiC). A truss structure concept design was developed, which could serve as optical bench for the scientific instrumentation of GAIA. It is lightweight and has a first eigenfrequency of 80 Hz. Also a concept design has been developed for the Basic Angle Monitoring (BAM) system of GAIA, which will measure 1 micro-arcsecond (μas) variations of the angle between the lines-of-sight of the two telescopes. For the design of these systems, contact mechanics is an important issue and therefore experiments have been conducted to obtain practical experience of the contact behaviour of SiC. This knowledge will be used in our project for a design of the BAM system. These experiments consist of friction experiments and experiments in which SiC tubes are bonded with several techniques like bolting, brazing and gluing.

1. INTRODUCTION

The GAIA mission is an ESA cornerstone mission, which will be launched in ca. 2010 to make a 3-D map of our Galaxy, by measuring the positions of stars with an accuracy of 10 μas and velocities with an accuracy of 1 kilometre per second. The satellite will consist of three parts, the solar shield, the service module and the payload module (PLM). The PLM is the module carrying the scientific instrumentation, which will include two astrometric telescopes with a focus length of 47 meters (m), and a spectrometer. The satellite will rotate around its longitudinal (z-)axis and thereby the astrometric telescopes will make a scanning motion. For optimal scanning efficiency and accuracy the angle between both telescopes fields-of-view (basic angle) will be 99.4°. A possible configuration of the BAM system is shown in Fig. 1.

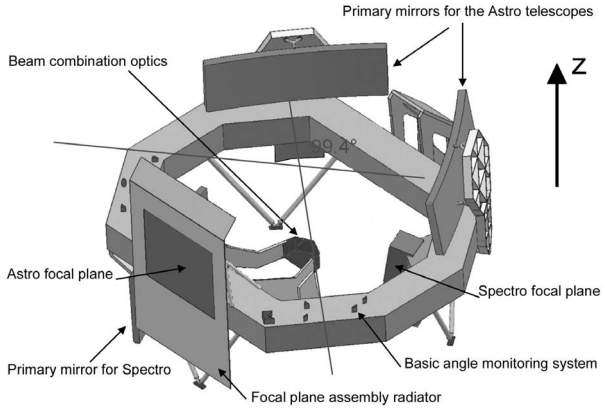

Fig. 1. Artistic impression of the GAIA payload module

To be able to construct a 3-D map of the Galaxy with μas-accuracy, the basic angle will need to be stable also to the μas-level. Therefore the optical bench, which supports the scientific instrumentation, will have to be extremely stable and at the same time stiff and lightweight. In section 2 attention will be paid to a possible design of an optical bench for GAIA.
It is, however, not sufficient to simply assume that the basic angle will be stable enough to achieve the μas-accuracy of star position measurement. Therefore, a BAM system will also be part of the payload module. The BAM system will measure with sub μas-accuracy the variations on the basic angle. This information will be used to correct for the basic angle variations during the star mapping calculations on Earth. Section 2 will also discuss basic ideas on this subject.
Section 3 focusses on experiments which have been performed up to this moment to study the characteristics of SiC are. These experiments have provided us with vital clues how to utilize SiC in highly stable systems. In section 4, the conclusions are summarized.
Section 5 focusses on future experiments, which will be performed.

2. SILICON CARBIDE STRUCTURES

In this section attention is paid to two subprojects concerning designing systems in SiC. The PLM of GAIA will be constructed for a large part in SiC. SiC is a ceramic material, with attractive characteristics. It has a high Young's modulus and low density and therefore a very high specific stiffness. Additionally, it has a low coefficient of thermal expansion (CTE) and high thermal conductivity and therefore a very low thermal sensitivity. It is also allegedly stable. Creep has not been seen in SiC to the nano-scale level [3, 4]. Of two types of SiC, a sintered SiC (SSiC) and a C/SiC (Carbon felt infiltrated with Silicon) and two metals, several material properties are shown in Table 1.

Table 1. Several materials properties

Material	ρ [g/cm^3]	E [GPa]	α [μm/m/K]	λ [W/m/K]
SSiC	3.1	420	2.5	180
C/SiC	2.6	248	1.2	170
Al alloy	2.7	70	24	220
Steel 316	7.8	205	17	45

The material, however, is also very hard, making it a lengthy and expensive process to grind or polish it or to saw or to bore it. Products should already be shaped in the green phase before conversion or sintering to SiC. Another aspect that should be taken into account when designing products in SiC, is that it is brittle and has much higher compressive strength than tensile and bending strength. This means that a ceramic material like SiC is preferably loaded compressively.

Two systems are considered here for design in SiC: the optical bench and the BAM system.

2.1 Optical bench for GAIA

In the design of the optical bench for GAIA stability is an important issue, since especially the basic angle between the fields-of-view of the astrometric telescopes should be stable. However, high stiffness and lightweight design are considered of equal importance, especially since the optical bench will have a diameter of 3 m and its behaviour will be crucial for the behaviour of the entire satellite during launch. Since the satellite cannot exceed a certain launch mass, limits have been stated for the mass of substructures, like the optical bench. The maximum mass for the optical bench has been stated to be 180 kg [1]. For the sizes, masses and locations of the scientific instrumentation educated guesses have been made. From this point a basic design is made.

Truss structures are very lightweight and stiff structures. It should be possible to make such structures in SiC, since SiC tubes are already made in rather large numbers and a variety of sizes for the high temperature process industry. Starting from a tetraeder, Finite Element (FE) analyses have been made, focusing on achieving a design with a first eigenfrequency, which is as high as possible and a mass that is as low as possible.

Fig. 2 shows a design of the space frame [2]. The frame is a double-walled truss structure. The total mass of the structure itself is ca. 120 kg and the structure consists of 189 tubes, with 5 different tube diameter and wall thickness combinations. The total mass of the supported optical instrumentation is about 600 kg.

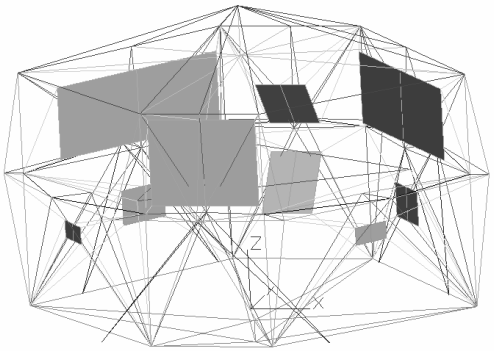

Fig. 2. FE model of the final spaceframe structure of the optical bench of GAIA. The panels represent mirrors of the telescopes and the focal plane assembly.

The first eigenfrequency of the truss structure made out of tubes of different diameters and lengths is 80 Hz. The truss structure is modelled with linear beams with cross sections, which have varying diameters and wall thicknesses. The nodes are assumed to be ideal and massless. The eigenmode is a total change of shape of the structure. It is not related to the eigenfrequency of the tubes. The eigenmode is a breathing mode in the Z-direction not affecting the basic angle.

The most challenging part of a space frame structure on both design and assembly are the nodes connecting the tubes. Special attention has been paid to the design of these nodes. The true coupling of the tubes at the node should be achieved at small distance from the node, because it is otherwise not possible to connect as many as ten tubes at each node. The characteristics of such a node should be: the possibility to assemble (especially the final tube), to disassemble, little transfer of moments into the nodes, high stiffness and stability of the contact and little extra mass.

From this analysis, experiments have been devised, in which SiC tubes are connected with different techniques, like tensioning, brazing and gluing. These experiments should give insight in the behaviour of SiC tubes in such connections. This will be discussed in section 3.

2.2 GAIA Basic Angle Monitoring system

The GAIA BAM system is an optical metrology system. The essence of the system is that it consists of two 'bars'. On bar 1 a point source and collimator sends a laser beam through an arrangement of beamsplitters and mirrors (Fig. 3). Two parallel beams are created which are sent through telescope 1 to create an interference pattern on the CCD camera (Fig. 1). Furthermore, two parallel beams are created, which are sent to bar 2. On this bar the beams are redirected, using mirrors, towards telescope 2. After travelling through telescope 2, these beams create a second interference pattern. If one telescope rotates with respect to the other, this results in a fringe shift of one pattern with respect to the other.

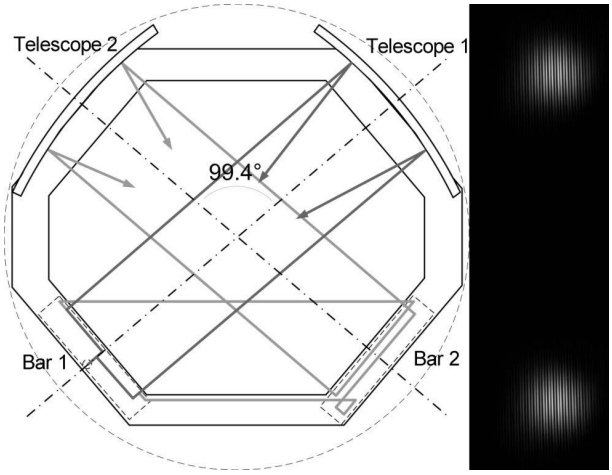

Fig. 3. Measurement principle and interference patterns

The optical configuration of the beamsplitters and mirrors is such that if bar 1 would rotate or move with respect to bar 2, this will not cause the interference patterns to shift with respect to each other. The alignment of the individual optical components is the key issue for the design of the mirrors and beamsplitters. This is threefold:

- the actions, which need to be taken to achieve alignment;
- the alignment of the component after having been subjected to launch vibrations and thermal cycling and;
- the alignment stability during measurements.

An optical component may not move more than 1 μm from its original position due to launch vibrations and thermal cycling and during measurements optical component may not move more than 1 picometer (pm) in a 6 hour period. This final requirement is considered the most stringent.

The considerations made in the design are: applying as little as possible grinding and polishing actions after sintering; making the mirror surface easily accessible for polishing; applying compressive loads only and as little as possible in the direction of the light path. The basic mirror and beamsplitter design is like shown in Fig. 4 and Fig. 5.

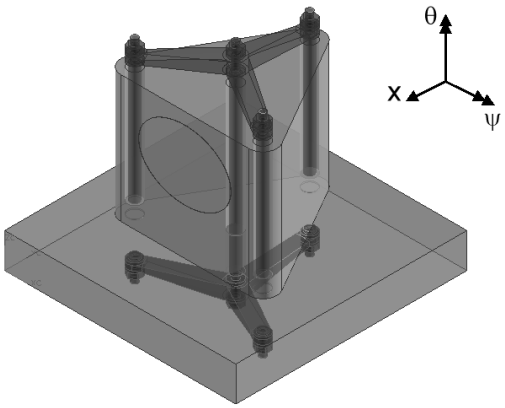

Fig. 4. 3-D view of the mirror mounted on a small plate

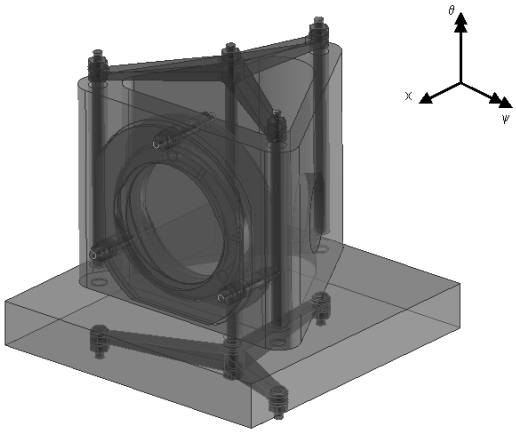

Fig. 5. 3-D view of the beamsplitter mounted on a small plate

The mirror and beamsplitter mounts are both mounted onto an optical bench, via three contact areas using a metal spider, which applies compressive loads through the contact areas of the mirror. Alignment is achieved by using an alignment mechanism which is removed from the mirror after alignment has been achieved and the spiders have been tensioned.

Experimentally, again the mechanical behaviour of contacts is important. Since the tensioning option has been chosen, the following questions need to be answered experimentally. What is the friction coefficient between both SiC bodies; what surface roughness should be used and; can a metallic interlayer reduce peak stresses and thus reduce the probability of failure? These questions are very closely related to the questions that can be asked for the connection of the tubes in the truss structure. Friction coefficient experiments have also been conducted for SiC on SiC

contacts and SiC on metal contacts. These experiments are also discussed in the next section.

3. EXPERIMENTS

3.1 Mechanical testing of connected Silicon Carbide tubes

Goals

The goal of the experiments performed with connected SiC tubes is to gain knowledge on the stability and stiffness of different connection methods with SiC tubes under a bending load.

Test specimens

There are 7 types of test-specimens, which are tested in this experiment.

Specimen 0 (Fig. 6) is a SiC (Hexaloy) tube, with a total length of 120 mm an outer diameter of 19 mm and an inner diameter of 14 mm, which is used for validation. The specimen has been diamond sawed from a SiC tube of 500 mm in length.

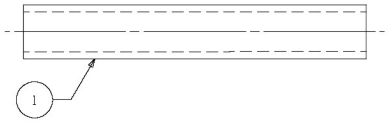

Fig. 6. Test specimen 0 with: SiC tube

Specimen 1 (Fig. 7) consists of two SiC tubes, with a length of 60 mm each, which are connected by a aluminium sleeve with a length of 30 mm and an outer diameter of 23 mm, which is glued over the SiC tubes with an epoxy Araldite AV 138. The SiC tubes have been sawed to length.

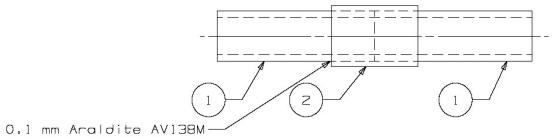

Fig. 7. Test specimen 1 with 1: SiC tubes sawed, 2: aluminium bus

Specimen 2 (Fig. 8) is a specimen consisting of two SiC tubes, with a length of 60 mm each, which are connected by brazing the ends together in a oven at 1300 °C with Cobalt Silicide ($CoSi_2$). The ends of the SiC tubes have a surface structure due to sawing. The SiC tubes have been sawed to length.

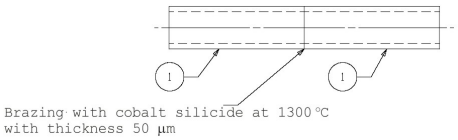

Fig. 8. Test specimen 2 with 1: SiC tubes

Specimen 3 (Fig. 9) consists of two SiC tubes, again with length 60 mm, which have been sawed to length. The tubes are connected on the ends with an aluminium foil with a thickness of 20 µm in between them. The tubes are compressed with an 8 mm. central bolt. The bolt has been tensioned with a force of 13 kN, which is equivalent with a contact pressure of 100 N/mm^2 between the SiC tubes.

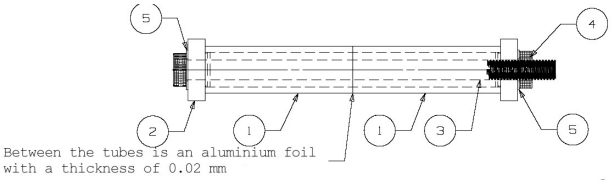

Fig. 9. Test specimen 3 with 1: SiC tubes sawed with aluminium foil of 20 µm between them, 2: aluminium ends, 3: 8 mm. Allen screw, 4: 8 mm. nut, 5: ring

The set-up is shown in Fig. 10. It is designed to tension the test specimens without introducing moments in the bolts and SiC tubes. Also the set-up is designed in such a way that the tensioning force can be controlled with an accuracy of ±100 N. The set-up consists of a hydraulic jack with a hand pump, which is hung onto a supporting structure. A compression drum is suspended on the outer shell of the jack.

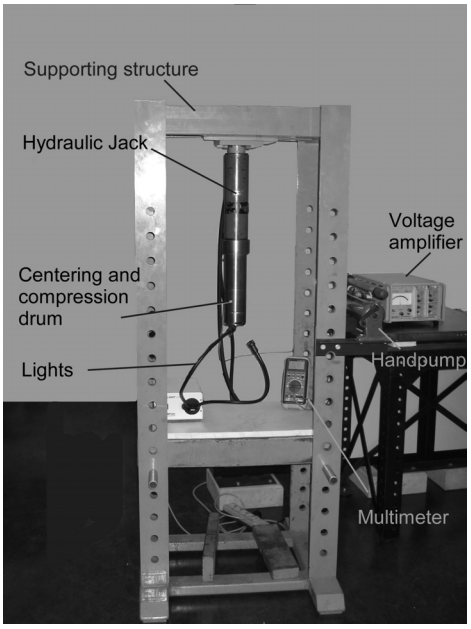

Fig. 10. Tensioning set-up

Inside the compression drum two cardans are fixed on both ends of a tension-compression loadcell, which can measure forces up to 20 kN. The cardan-loadcell-cardan combination is suspended on the plunger of the hydraulic Jack. The loadcell is a strain gauge type loadcell. The compression drum has been equipped with a slit, to provide a passage for the wiring of the loadcell to the amplifier. The amplifier is then connected with a multimeter to read the voltage. The amplifier can give -5V to +5V output and can have a sensitivity of 0.05 to 10 mV/V. The loadcell has been calibrated to give 3.090 V output at 2 mV/V sensitivity at a load of 13 kN.

The lower cardan, which is attached to the loadcell, has an 8 mm. hole in the bottom in which the bolt or threaded end of the test specimen can be screwed. In the lower end of the compression drum, a slit has been milled (Fig. 11). The nut on the top of the specimens has small holes around its perimeter in which a pin can be stuck through the slit and which can be used to screw the nut, when the bolt is tensioned by retracting the plunger. When the plunger is retracted, the aluminium end will be pressed against the compression cylinder. The nut will be free from the aluminium end, so that it can be turned with the pin, until it rests against the aluminium end again. Two flexible lights are directed towards the slit of the set-up to create light, which can help with the assembly of the set-up with test specimens.

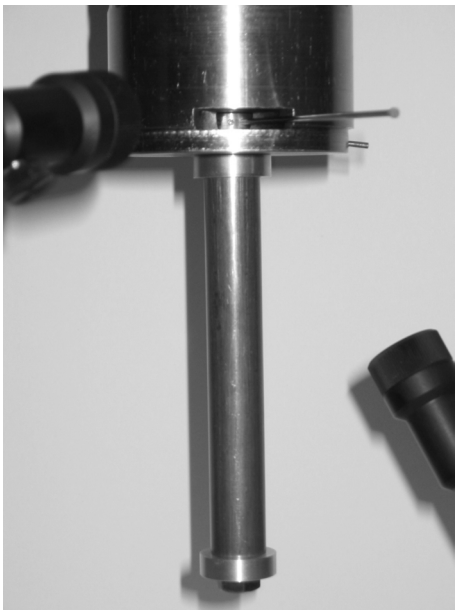

Fig. 11. Close-up of a test-specimen fixed to the tensioning setup

During the tensioning of the 7 samples of specimen 3, 3 samples failed in spite of the efforts made to provide contact conditions with only compressive load. An example is shown in Fig. 12.

The specimens failed on one side, indicating that still a bending moment must have been present in the specimen, loading the contact area unevenly.

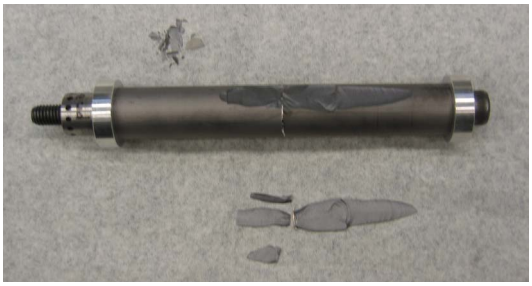

Fig. 12. Failed sample of specimen 3

Specimen 4 (Fig. 13) is a specimen similar to specimen 3, with this difference that the connected ends have been grinded to a roughness of R_A = 0.3 μm. No foil is applied between them.

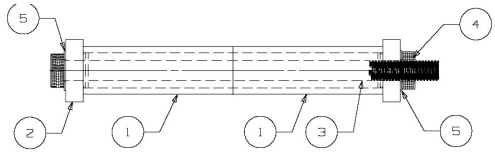

Fig. 13. Test specimen 4 with 1: SiC tubes polished to RA = 0.3 μm on contacting ends, 2: aluminium ends, 3: 8 mm. Allen screw, 4: 8 mm. nut, 5: ring

For assembly and tensioning, the same set-up has been used as for specimen 3. No specimens failed in this case.

In specimens 5 (Fig. 14) and 6 (Fig. 15), an insert with a length of 30 mm is glued in one SiC tube of length 60 mm with Araldite AV 138. In specimen 5 the ends of the tubes have a sawed finish and an aluminium foil (20 μm) is applied between them. A bolt is screwed into the insert and the tubes are again tensioned with a 13 kN force in the bolt, equivalent to a contact pressure of 100 N/mm^2. Specimen 6 is similar to specimen 5, but the ends have been grinded like in specimen 4 and no foil has been applied between them.

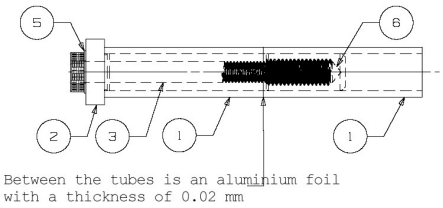

Fig. 14. Test specimen 5 with 1: SiC tubes sawed with aluminium foil of 20 μm between them, 2: aluminium end, 3: 8 mm. threaded end, 5: 8 mm. nut

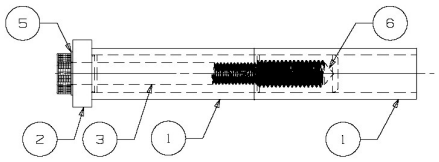

Fig. 15. Test specimen 6 with 1: SiC tubes polished to RA = 0.3 μm on contacting ends, 2: aluminium end, 3: 8 mm. threaded end, 5: 8 mm. nut

For specimens 5 and 6 again the tensioning set-up shown in Fig. 10 was used. With specimen 5, 2 of 7 samples failed during tensioning, one of which is shown in Fig. 16. With specimen 6 also one sample failed, but not due to bending moments and peak stresses at the contact, but due to an air bubble in the Araldite adhesive, causing the shear stress to be uneven, resulting in a pulled out insert. The air bubble could have been avoided if the inserts would have been equipped with small slits, which would have better distributed the adhesive.

Fig. 16. Failed sample of specimen 5

Fig. 17. Failed sample of specimen 6

The failed specimens of specimens 3 and 5 provided insight in what aspects should be taken into account when two SiC bodies are in contact under high compressive load:

- Polishing the contact areas works.
- It seems that sawing of the test specimens introduced a too large roughness for the 20 μm thick aluminium foil to handle for some specimens. However, most specimens survived the tensioning without visible damage, implying that the aluminium did its job. Sawing also creates microcracks in the surface which typically extend to a depth equivalent to the size of the diamond grains on the saw blade (75 μm). Especially cracks, which extend perpendicularly to the sawed surface, are harmful. Also, sawing introduces a very repetitive roughness pattern, which might have negative results for the failure strength of the specimens. A solution is to grind the specimens with a diamond grain of 30 μm. The microcracks introduced by the sawing should be grinded to a depth of 45 μm to reduce the size of the microcracks. This should be sufficient with an intermediate aluminium layer of 20 μm.

The 4-point bending set-up

The set-up is an equivalent of a 4-point bending set-up. The set-up has however been adapted to be able to handle the shape and size of the specimens. In Fig. 18, a schematic representation of the set-up is shown. Since the specimens are tubular, they are placed in V-blocks, to prevent them from rolling away. Because the expected loads are rather high, up to 10 kN, the specimens are not contacting the V-blocks with point contacts, but with line contacts, so that the contact stress is reduced. However, bending should remain possible, which is why the V-blocks are equipped with elastic hinges, so that the V-blocks will rotate with the bending of the specimen.

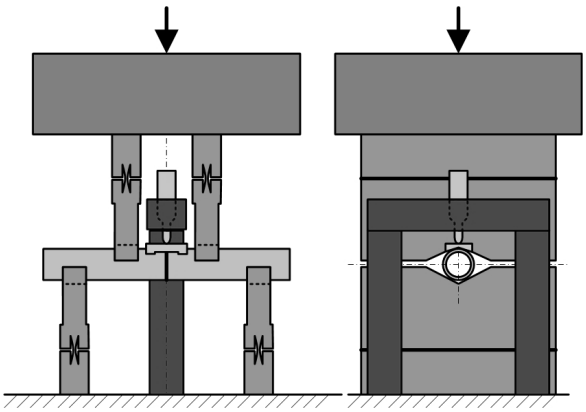

Fig. 18. Schematic representation of the 4-point bending set-up

Since the specimens have a large tolerance (0.5 mm) on their radius, roundness and straightness, the V-blocks are fixed to the tensile testing bench with one fitted bolt in the centre, so that the set-up becomes self-aligning and line-contacts can be assured.

The two upper contacts are also V-blocks and they are pressed down by the stamp of a tensile testing bench.

The tensile testing bench is the Zwick Z010 bench, which can give a 10 kN force with an accuracy of 1 N. The header position can be measured with 10 μm accuracy. The Zwick Z010 is driven using computer control. Software can be written in a special program, which can drive the bench in a reproducible manner.

The set-up is furthermore equipped with a +/- 0.5 mm inductive displacement sensor like shown in Fig. 18, which can measure displacements under 0.1 mm with an accuracy of 0.6 μm and above that with 1.5 μm accuracy. The displacement sensor is interfaced with a Siglab box, which converts an analog voltage to a digital voltage, which can be sampled and saved in a data file.

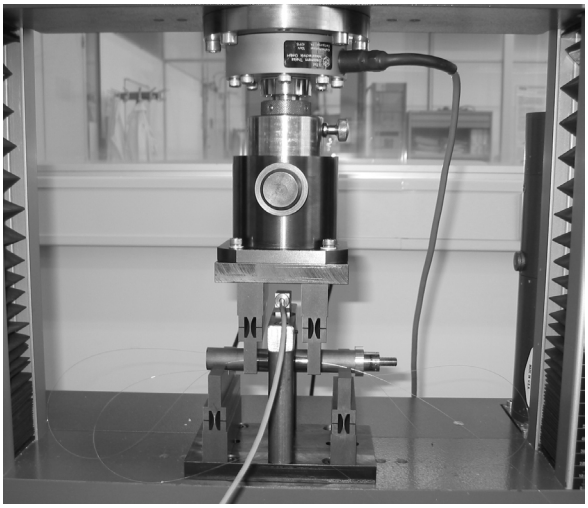

Fig. 19. Close-up of the 4-point bending set-up with added displacement sensor and specimen with attached Fibre Bragg gratings

The goal of these experiments is to gain knowledge of what happens at the contact area under cyclic loading. Therefore, a third measurement system used for the cyclic 4-point bending experiments is the Fibre Bragg Gratings (FBGs). FBGs are strain gauges. However, these FBGs do not function by creating a change in electrical resistance due to the strain of the gauge, but by a change in the wavelength of the light reflected by the grating which has been build in the optical fibre. In case the circumstances are stable one microstrain will cause a wavelength change of 1 pm. The FBGs are ideally attached to the specimen by using an adhesive like Araldite. However, in that case the fibres would not be removable. Since a large number of specimens will be tested, the choice has been made to attach the gratings to the specimens by means of Kapton adhesive tape. Three fibres are attached to the specimen, all in the axial direction of the tube. Two fibres are taped, one on either side, and one is taped on the underside. Due to the bending of the specimen, the latter will measure the largest strain and the strain of the two other fibres will be close to zero, unless the two connecting tubes would shift with respect to one another. It would have been more logical to have taped the fibres on the sides at an angle with respect to the tube axis. However, experience in taping the fibres to the specimens has learned that it is very difficult to apply the fibres correctly (under slight tension), due to the rather small radius of the tubes.

Method

The 4-point bending experiments consists of 2 stages:

- Experiments up to failure, which establish a safe force margin for the subsequent cycling experiments. Of each specimen, one sample is prepared with Teflon tape at the contacts to fill out roughness variations. It is then carefully pre-aligned to make sure that equal forces exist at all contacts. The displacement sensor and FBGs are not used in these experiments. From pre-alignment position the crosshead is moved down with a speed of 0.01 mm/s, until a force is measured of 7.5 kN or until a sudden reduction in force of 50 N in 1 second occurs. The force, time and displacement of the crosshead is saved every 0.1 μm. In case of fracture, a small investigation is made on what could be the reason for failure.

- Cycling experiments, which should give insight in the behaviour of the specimens in the contact area. Each sample is prepared by applying the three FBGs. The sample is then carefully placed on the lower V-blocks. In the next step the displacement sensor is placed in contact with the specimen, using another small V-block on the specimen. The displacement sensor is calibrated to 0 with an accuracy of 0.1 μm. This is taken as the zero displacement point. This is followed by moving down the crosshead to achieve pre-alignment. The measurement is then initialised. The crosshead is moved down from pre-alignment position with a speed of 0.01 mm/s, until a force is measured of 2 kN and then moved up to a load of 1 kN and back again to 2 kN until 10 cycles have passed (Fig. 20). The force, time, the displacement of the crosshead, the wavelength of the FBGs and the displacement of the inductive sensor are saved with a sampling frequency of 50 Hz.

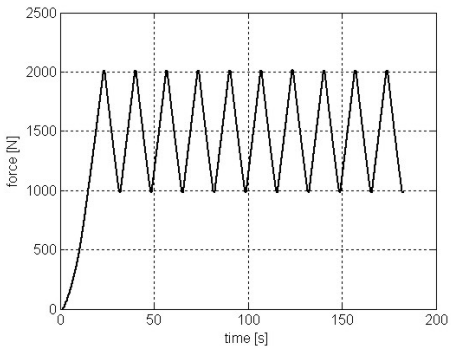

Fig. 20 Time-force plot of the cyclic loading experiment

For each sample the measurement is repeated 4 times after the first pre-alignment and then the sample is pre-aligned again and the measurement is repeated another 3 times. Also of each specimen, 3 samples are measured. This will give sufficient information on the repeatability of the measurement on one sample.

Results of failure experiments

Most specimens did not fail completely during the failure experiments. Specimen 1, specimen 2 and specimen 6 failed. Specimen 1 broke at the lower right V-block on the inside. Although the imprints on the Teflon tape (Fig. 21) look very nicely rectangular, the pressure on the inner edge of the V-block must have been too high. In a further examination under the microscope, it was found that on the side of the specimen that did not fail, the Araldite adhesive did already fail at the edge of the aluminium sleeve due to shear (circle in Fig. 21). The fracture pattern of the adhesive is drawn schematically in Fig. 22. The cracks show a switch in direction between the bottom and the top of the tube. This is due to the fact that on the bottom the shearing stress is in the opposite direction of the shearing stress in the top part of the specimen.

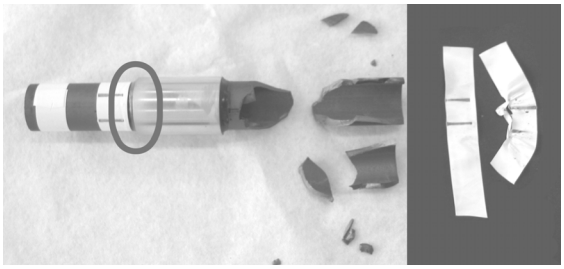

Fig. 21. The fractured specimen 1 sample 1

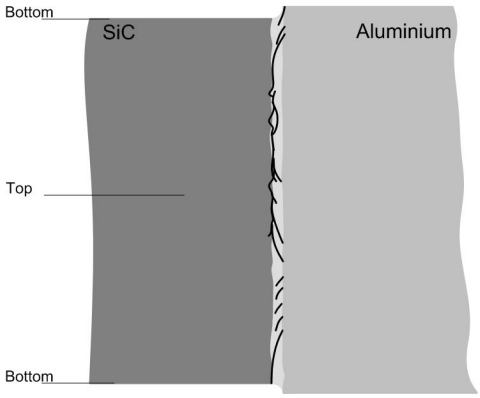

Fig. 22. Fracture pattern in the Araldite adhesive. The perimeter of the tube is laid out.

Specimen 2 has failed at about 2400 N, at which moment the maximum stress would have been 130 N/mm^2. The specimen has a clean fracture of the braze itself. On both brazed ends, the braze remains are visible (Fig. 23).

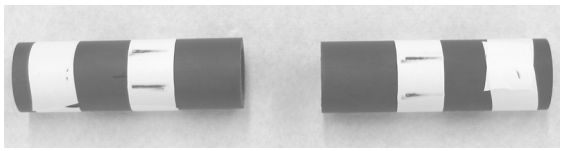

Fig. 23. Fractured specimen 2

Specimen 6 failed at already 2200 N. A photograph of the fractured specimen still in the set-up (Fig. 24) shows that the specimen has failed at the lower right V-block.

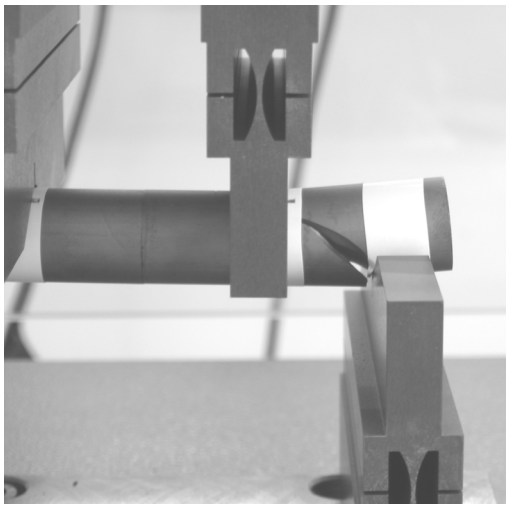

Fig. 24. Fractured specimen 6 zoomed in at the lower right V-block

The fractures are clearly visible. In a close examination, long fractures seem to originate into both tubes from the contact area on the top of the specimen, where the compressive stresses are highest. However, the fact that the tubes broke in two with fracture lines at the upper and lower line contacts, can lead to believe that the long fractures might be caused by the V-blocks themselves. It is not clear which is the correct conclusion.

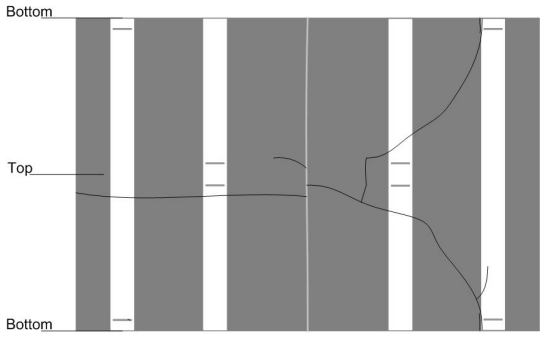

Fig. 25. Fracture pattern in the SiC tubes of specimen 6. The perimeter is laid out

The other tensioned specimens (3, 4 and 5) have been subjected to the load, without any fractures. However, when the specimens were examined under the microscope, they showed fissures with patterns very similar to specimen 6.

In conclusion, the cyclic loading experiments will load to a maximum force of 2000 N to avoid fissure formation. A minimum load of 1000 N is taken, to take out any non-linear behaviour of the set-up itself.

Results of the cyclic loading experiments

The results can be divided in the results for each separate measurement device:

- With respect to the force measurement the following observations can be made. The initial force is manually achieved with an accuracy of -10 to +10 N. The maximum and minimum forces measured indeed have a dispersion of 1 N. The dispersion is independent of the specimen, of the sample number, or the experiment number. The maximum force is in average 2016 N, which is 16 N above the stated maximum force of 2000 N by the interface software of the Zwick tensile bench. In the maximum force, a dependency is observed in the cycle number. For all measurements the maximum force of the first cycle is 1 N lower than for the other 9 cycles. The minimum force is on average 986 N, which is 14 N below the stated minimum force of 1000 N by the interface software. For the minima, no dependency of the cycle number is observed. The offset in force is caused by a very slow force controller in the interface software.

- The path maxima and minima measurements are shown in Table 2. The results show that the maxima and minima of the crosshead path have a higher standard deviation than the tensile bench accuracy. This is caused by the inaccurate pre-alignment force. Therefore, also the difference between the maximum and minimum path of each cycle is computed, shown in the two most-right columns. These show that the average displacement is independent of the specimen and the standard deviation is below the measurement accuracy of the tensile bench.

Table 2. Maxima and minima measurements of the crosshead path

Specimen	Maximum path		Minimum path		Peak-to-valley path	
	μ	σ	μ	σ	μ	σ
All	0.233	0.024	0.150	0.024	0.080	0.002
0	0.239	0.022	0.150	0.022	0.080	0.001
1	0.222	0.010	0.140	0.010	0.080	0.001
2	0.214	0.018	0.133	0.018	0.080	0.002
3	0.229	0.022	0.147	0.021	0.080	0.001
4	0.243	0.028	0.161	0.027	0.080	0.002
5	0.227	0.020	0.144	0.021	0.081	0.002
6	0.260	0.010	0.176	0.011	0.082	0.001

One other observation has been made with respect to the maximum and minimum path of the crosshead. In each measurement the maximum and minimum paths increase with 2 or 3 μm during the cycles. This could be caused by the limit of the repetitiveness of the tensile bench crosshead position or it could be caused by slight remaining hysteresis of the 4-point bending set-up.

When examining the maximum-minimum paths of the samples per specimen, it can be observed that an individual sample does not affect the measured path maximum – minimum with a difference larger than the accuracy of the path measurement of 2 μm.

- Table 3 shows the averages and standard deviations for the displacement sensor measurements. The maxima and minima displacements are smaller than the displacements measured by the tensile bench itself, which can be explained by the fact that the deformation of the upper part of the set-up itself is not measured. For the maxima and minima of the displacement, the dispersion is caused by small pre-alignment differences. The peak-to-valley displacement of one cycle has a dispersion in the same order as the accuracy of the displacement sensor. The dispersion of an individual sample is of the same order as for all specimens.

The peak-to-valley displacement of specimens 2, 5 and 6 is 1 μm larger than for the other specimens.

Table 3. Maxima and minima measurements of the displacement sensor

Specimen	Maximum displacement		Minimum displacement		Peak-to-valley displacement	
	μ	σ	μ	σ	μ	σ
All	0.037	0.006	0.022	0.005	0.014	0.002
0	0.036	0.002	0.021	0.001	0.014	0.001
1	0.037	0.002	0.023	0.001	0.014	0.001
2	0.038	0.005	0.022	0.004	0.015	0.001
3	0.036	0.004	0.022	0.003	0.014	0.001
4	0.035	0.002	0.021	0.002	0.014	0.001
5	0.042	0.003	0.027	0.003	0.015	0.001
6	0.042	0.003	0.027	0.003	0.015	0.001

- Table 4 shows the averages and standard deviations for the FBG measurements of the lower fibre, which exhibits the largest strain due to the bending of the tubes. Like for the path of the crosshead the spreading of the maxima and minima of the wavelength change is large. This can also partly be caused by the large dispersion of the initial force. However, this effect cannot be as large since this force variation is still only 1 % of the minimum force peaks. Another effect is considered more important. The accuracy, with which the specimens have been aligned with the fibre at the lowest possible point, may not have been ideal. This also explains why the standard deviation of the peak-to-valley wavelength is not lower than the standard deviation of the individual maximum and minimum wavelength changes.

Table 4 Maxima and minima measurements of the wavelength change

Specimen	Peak strain (x 10^{-3})		Valley strain (x 10^{-3})		Peak-to-valley strain (x 10^{-3})	
	μ	σ	μ	σ	μ	σ
All	0.134	0.047	0.044	0.015	0.086	0.031
0	0.134	0.007	0.046	0.004	0.083	0.004
1	0.042	0.022	0.016	0.008	0.026	0.013
2	0.121	0.029	0.039	0.014	0.077	0.015
3	0.170	0.027	0.054	0.006	0.110	0.020
4	0.134	0.011	0.046	0.006	0.084	0.006
5	0.187	0.037	0.053	0.018	0.125	0.020
6	0.146	0.014	0.048	0.007	0.093	0.007

Another effect which has been observed in the maxima and minima of the wavelengths is a drop in wavelength during the 10 cycles. The averages of the drops are higher when the average wavelength change is higher. The drop in wavelength is generally of the same order as the dispersion of the results and rather predictable.

Table 5 Wavelength drop of maxima and minima measurements after 10 cycles

Specimen	Peak strain (x 10^{-3})		Valley strain (x 10^{-3})		Peak-to-valley strain (x 10^{-3})	
	μ	σ	μ	σ	μ	σ
All	0.022	0.009	0.016	0.006	0.006	0.003
0	0.022	0.004	0.017	0.003	0.006	0.001
1	0.005	0.004	0.003	0.003	0.001	0.001
2	0.023	0.005	0.016	0.004	0.006	0.001
3	0.027	0.005	0.019	0.004	0.007	0.003
4	0.021	0.003	0.016	0.002	0.005	0.001
5	0.032	0.005	0.021	0.004	0.010	0.001
6	0.023	0.004	0.017	0.004	0.006	0.001

When examining the maximum-minimum wavelengths in a scatter plot (Fig. 26), it follows that the wavelength change of specimen 1 is significantly smaller than the change for the other specimens. This is due to the fact that the fibres have been attached in a different manner, because the aluminium bus is too small for the fibres. The FBGs have therefore been attached partly over the aluminium and partly over the SiC.

Another aspect, is that the values for specimens 3 and 5 have a mean value that is larger than for the other specimens, although the standard deviation for these specimens is also larger than for the other specimens. This can be explained by the fact that specimens 3 and 5 are equipped with an aluminium foil, which has lower stiffness than the SiC tubes.

It also appears that there is a difference between specimens 3 and 4, which are the compressed tubes without the insert, and specimens 5 and 6, which are the compressed tubes with the insert. The wavelength change for the latter two is somewhat higher (although hardly significant), but can be explained by the shear strain of the Araldite adhesive used to glue in the insert.

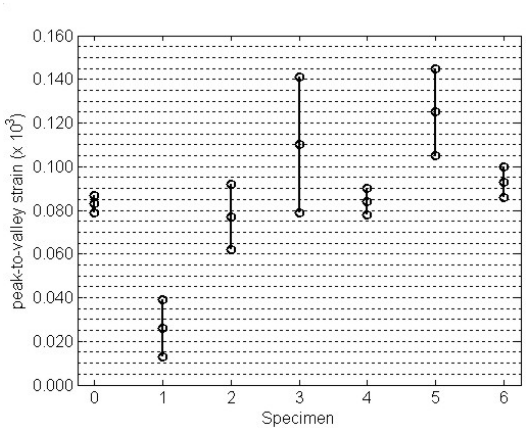

Fig. 26. Scatter plot of the maximum-minimum wavelengths for each specimen

- Fig. 27 shows a characteristic plot of the force and the strain of the lower FBG. The strain for the FBG's on the sides also show this behaviour, be it with a smaller magnitude. The observation that can be made is that the strain of the FBG tends to reduce more when the force decreases, than the strain will increase during the increase of the force. This effect is strongest in the first loop and is most likely caused by the fibre being relaxed by the Kapton tape, which was already mentioned above.

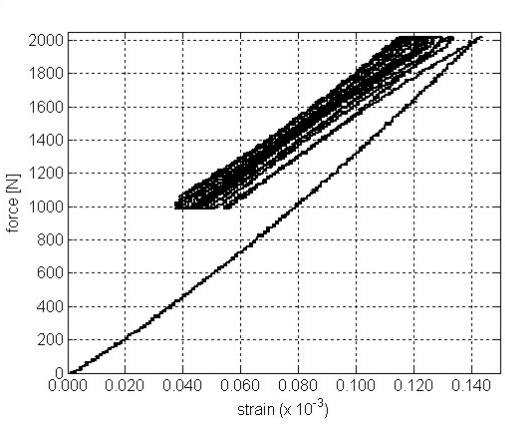

Fig. 27. Force-lower FBG strain plot of specimen 0

The force against the displacement plot, measured by the inductive sensor, seems to show very slight hysteresis (Fig. 28). However, this apparent hysteresis is smaller than the accuracy of the displacement sensor, and thus it should be concluded that no hysteresis is measured within the measurement accuracy.

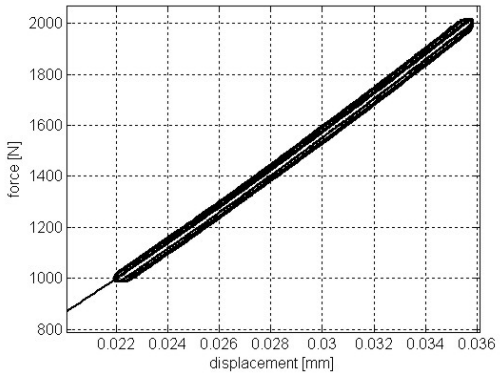

Fig. 28. Force-displacement plot of specimen 0

All specimens show that same relaxation effect shown in Fig. 27, which prevents any measurement of the hysteresis of the contacting tubes themselves. The conclusion can be drawn that to within measurement accuracy of ca. 10^{-5} strain, no difference has been observed in the mechanical behaviour of the contacted tubes. Therefore, they are all stable in a bending load of 2 kN to within 10^{-5} strain.

3.2 Friction experiments

Pin-on-disc experiments have been performed with different SiC-SiC and SiC-metal contacts

Goals

The goal of the pin-on-disc experiments is to determine the friction coefficients of different SiC-SiC and SiC-metal contacts under high compressive loads of 50 MPa at room temperature.

Very little information exists on the friction coefficient of SiC-SiC or SiC-metal contacts at room temperature and certainly not at lower temperatures. Most friction experiments have been performed at extremely high temperatures of 1300-1800 °C or have been focused on the wear behaviour of SiC [5, 6, 7].

Method

In order to determine the friction coefficient of SiC-SiC and SiC-metal contacts with SiC, pin on disc experiments have been performed with a disc of either SSiC or C/SiC, and a pin of either aluminium, stainless steel, SSiC or C/SiC. The disc has a diameter of 76 mm and a thickness of 15 mm. The pins are 5 by 5 mm^2 with a length of 11 mm. The contacting surface of the pins has been made conform with the radius of the disc in order to make a good flat-on-flat contact. The pin is pressed against the disc with a normal force of 1.25 kN shown schematically in Fig. 29. The disc is rotated with a speed of 0.48 rad/s, or 0.02 m/s at the contact. With a torsion meter the torsion can be measured, this data could be used to compute the friction coefficient.

The surface roughness of the pins and the discs is 0.3 μm R_A.

Fig. 29. Pin on disc experiment

Results

The friction coefficients are shown in Table 6. The accuracy of the results is ±0.05 (-).

Table 6 Friction coefficients

Ring / Pin	SSiC	C/SiC
SSiC	0.45	
C/SiC	0.50	0.48
Aluminium	0.60	0.57
Stainless steel	0.48	0.44

With the C/SiC disc, all materials showed a small peak at a coefficient of friction of 0.25. This is attributed to the porosity of the C/SiC, which is about 20 %. The SSiC has a porosity of only 3 %.

The results also show that the aluminium on SiC contact resulted in a higher friction coefficient, than in the other contacts. The discs showed an aluminium residue after the experiment, which implies that the higher friction coefficient is caused by transfer of aluminium.

In the initial experiments, the normal load was 2500 N. This load was reduced, because the SiC pins did not withstand the bending loads, which were caused by a limited stiffness of the clamps in the tribometer.

4. CONCLUSIONS

Experiments have been performed with SiC with special focus on the behaviour of SiC to SiC contacts and SiC to metal contacts.

The methods of joining SiC tubes have all been rather successful. 2 of 7 specimens which have been pressed

together using tensioned bolts fractured. This provides insight in surface treatment. Polishing the contact areas works, because none of the specimens with polished contact areas has fractured.

One specimen has fractured due to bad adhesion of the Araldite to the SiC tubes. This is ascribed to the method of gluing the tubes. Canals should have been present to make sure that the adhesive would have flowed everywhere.

It seems that sawing of the test specimens introduces a too large roughness for the 20 μm thick aluminium foil to handle for 2 of 7 specimens. However, most specimens have passed the tensioning without visible or hearable damage, implying that the aluminium did its job.

The bending experiments up to failure, learn that the maximum stress the $CoSi_2$ braze can withstand is 130 N/mm^2.

The bending stiffness of the specimens measured at forces up to 2 kN, is not influenced by the different methods of joining two SiC bodies.

The displacement measured over 1 kN, is 0.014 mm, which corresponds to a bending stiffness of $7.0 \cdot 10^7$ N/m.

Nevertheless, the lower FBG of specimens 3 and 5 show an increased strain on average of $0.03 \cdot 10^{-3}$ with respect to the specimens 4 and 6, which is attributed to the lower stiffness SiC-SiC contact with the aluminium foil in comparison to the bare SiC-SiC contact.

No conclusions can be drawn on a possible hysteresis in the contact area of the SiC tubes, because the Kapton tape, which fixed the FBGs to the specimens, did exhibit relaxation.

The friction experiments show that the friction coefficient of SiC on SiC and SiC on steel, with a roughness of 0.3 μm R_A and 50 MPa load, is around 0.5. The friction coefficient of aluminium on SiC is higher with a value of 0.6. This was attributed to the transfer of aluminium to the SiC surface during the experiment.

5. FUTURE EXPERIMENTS

Successive experiments will be conducted for the friction experiments in the near future. Since the GAIA satellite will fly in deep space at low temperatures, we will measure the friction coefficient of SiC to SiC contacts and SiC to metal contacts at low temperature (-50 °C) .

Other experiments will be focused on the thermal behaviour of two contacting SiC bodies. Measurements will be performed to measure thermal contact conductance of two SiC bodies in contact in vacuum. In these experiments the influence on the thermal contact conductance of several aspects will be investigated. These are:

- normal contacting load,
- influence of contact radii,
- the influence of interstitial coatings, which should improve the thermal contact conductance.

The goal is to optimise the thermal contact conductance as much as possible.

6. ACKNOWLEDGEMENTS

We would like to make acknowledgements to Edwin Stam of TNO Science and Industry, who has performed the friction measurements. Also the Netherlands Agency for Aerospace Programmes NIVR is acknowledged for funding this research.

7. REFERENCES

1. GAIA SLTRS project team, *GAIA system level technical reassessment study final report* (2002), Astrium, France

2. W.J. Berkhout, M.K. Schalkx, *Herontwerp Optical Bench* (2003), internal report in Dutch, Technische Universiteit Eindhoven, Eindhoven, The Netherlands

3. Marschall, C.W., Maringer, R.E. *Dimensional Instability: An introduction* (1977). 22nd edition, Pergamon Press, New York, ISBN 0-08-021305-7

4. Shih, C.J. et al. *Damage evolution in dynamic deformation of silicon carbide* (2000). Acta Materialia 48, p. 2399-2420.

5. Dong, X., Jahanmir, S., Ives, L.K. *Wear transition diagram for Silicon Carbide.* Tribology International, vol. 28, no. 8, pp. 559-572, 1995

6. Yust, C.S., Carignan, F.J. *Observations on the sliding wear of ceramics.* ASLE Transactions, vol. 28, no. 2, pp. 245-252, 1984

7. Gee, M.G., Matharu, C.S., Almond, E.A., Eyre, T.S. The measurement of sliding friction and wear of ceramics at high temperature. Wear, vol. 138, pp. 169-187, 1990